Chapter 5

Computer model results.

In this chapter a numerical simulation of the fluid annulus has been used to test certain ideas concerning the ζ-circulation. The model is described in §5.1 and the results compared with experimental measurements in §5.2. In §5.3 a simulation is used to check the validity of the scaling analysis of §1.2.2. The ζ-circulation is investigated in §5.4. One mechanism is proposed in §5.4.1 and tested in §5.4.2. It is found that the centrifugal force appears not to play a part in the formation of the ζ-circulation. A further mechanism is suggested and tested in §5.4.3. The conclusions of the investigations are given in §5.5.

5.1 The computer model.

The numerical model of the annulus used was that of *James et al (1981)* and *Hignett et al (1985)*. It is a grid–point finite difference formulation based on the (non–hydrostatic) Navier–Stokes equations for incompressible baroclinic flow in a Boussinesq fluid. The standard resolution of the model is 16 (vertical) × 16 (radial) × 64 (azimuthal) points; the grid is stretched in the (r, z)-plane to resolve boundary layers. The performance of the model in comparison with experimental results, applied to unblocked annulus flows, is discussed in *White (1988)*. The dynamical equations used by the model are given in *Hignett et al (1985)* where

the centrifugal term discussed below is shown explicitly (see *Table 5.2* below). The numerical and experimental investigations used identical geometries.

The model was modified to include a fully blocking thermally insulating radial barrier by A.A.White (*private communication*). The boundary conditions on the sides of the barrier amount to a 'no–slip' condition (i.e. $u, v, w = 0$ at the sides of the barrier), however the implementation of the boundary conditions at the barrier was complicated by the use of two sets of grid points, each displaced relative to the other. The barrier was placed on one of the grids, and then an extra set of 'fictitious' points introduced on each side of the barrier which formed part of the second grid. This meant that the boundary conditions could be applied to the quantities calculated on the second grid at the location of the barrier by interpolating between the grid points. In effect the model sees two barriers, one at each of $\phi = \pm\pi$. For the second grid, with azimuthal spacing $\Delta\phi$, the grid points nearest the barrier were at $\phi = -\pi \pm \Delta\phi/2$ and $\phi = \pi \pm \Delta\phi/2$, so that boundary conditions for the barrier could be applied between those points.

P.L.Read (private communication) has raised certain doubts as to whether the diagnostics routines have correctly interpreted the model data near the barrier, because of the 'fictitious' points the model used (see above). However he believes that the velocity and temperature fields should be unaffected by this problem.

5.2 Comparison of model results with experimental data.

This thesis does not attempt to verify the numerical model in any detail, however it seems advisable to compare the model results with experimental measurements taken using the similar system described in chapter 3.

Figure 5.1 shows velocity results from the numerical simulation displayed in a similar format to that of the experimental results.

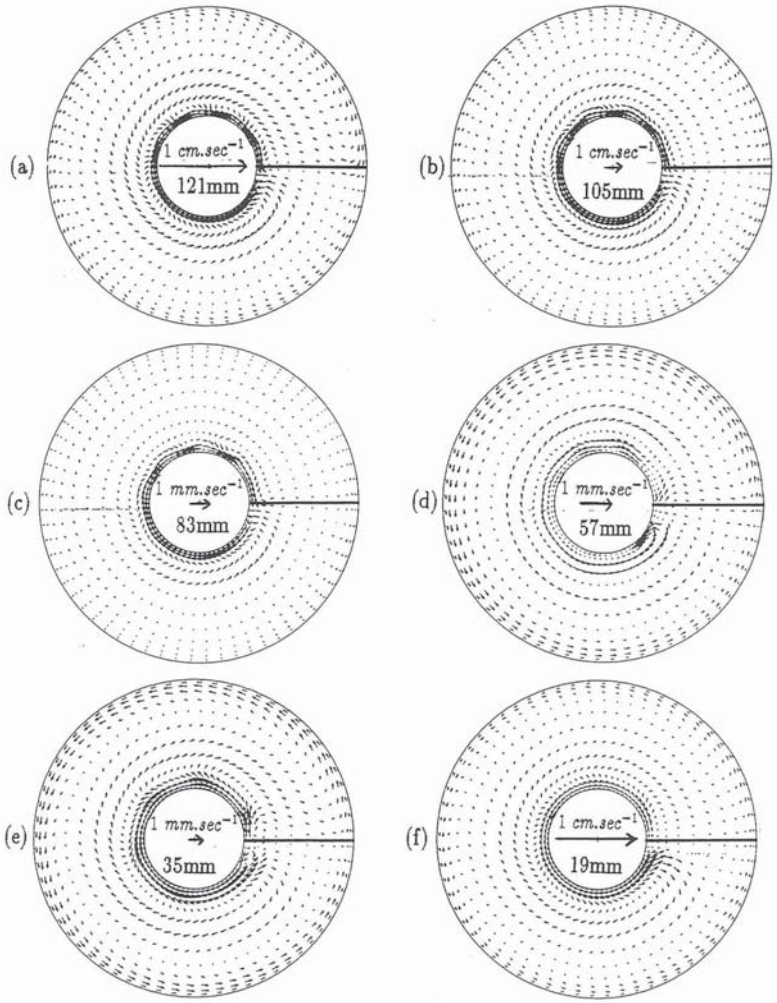

FIGURE 5.1: Computer model simulation of flow in a fully blocked annulus of constant depth, $d = 140\ mm$. Horizontal velocity results in an (r, ϕ)-plane. The solid line in the three o'clock position indicates the location of the barrier. The central arrow in each case represents a velocity of 1 $mm.sec^{-1}$ or 1 $cm.sec^{-1}$ as indicated. The heights of the (r, ϕ) cross-section above the base of the annulus are also given in the centre of each diagram. Results from run 751, $\Omega = 1.2\ rad.sec^{-1}$, $\Delta T = 4\ K$. Radial inflow can be seen near the top (a), and radial outflow near the bottom (f). Prograde flow can be seen by the outer wall in (d)-(f). Some distance from the inner wall retrograde flow can be seen in (d)-(f). The strong flow close to the inner cylinder in all the plots is the spurious motion mentioned in the main text.

The horizontal velocity data is shown, where possible, at similar heights to the measurements made in the experiments. *Figure 5.2* shows experimental velocity measurements at values of Ω and ΔT close to those of *Figure 5.1*. The experimental velocity measurements were not reprojected onto a regular grid, in order to avoid the possible errors associated with the least squares fitting routine, which are described in §2.2.5.

Bearing in mind the differences in heights that the horizontal velocity data are shown at, the velocities shown in *Figures 5.1* and *5.2* should be almost identical. In general terms both figures show radial inflow near the top of the annulus and radial outflow near the bottom. Also at mid to lower regions there is prograde flow by the outer wall, and the magnitudes of the fluid velocities appear to be broadly similar. However close inspection reveals differences. The most obvious of these is the strong flow which appears by the inner cylinder in *Figure 5.1*. While it could be argued that there are few indications of the velocity close to the inner cylinder in *Figure 5.2*, in general, the numerical and experimental results appear to disagree in this region, particularly in the lower parts of the annulus. It is just possible that *Figures 5.1(b)* and *5.2(b)* agree, but in the simulation results there is prograde motion by the inner cylinder in (d) and (e), while the experimental results show retrograde motion in (c) and (d), over a broadly similar range of heights. It seems likely that the numerical simulation is having difficulty resolving the fluid motions in the region next to the inner cylinder.

Figure 5.3 shows velocity and temperature results for the same run as *Figure 5.1*. The mean radial velocity results in *Figure 5.3 (a)* appear to be quite similar to those in *Figure 3.5*. Also, apart from the spurious motions by the inner cylinder, *Figure 5.3 (b)* seems similar to *Figure 3.6*. It is worth noting that *Figures 5.3 (a)* and *(b)* agree quite well with the conducting barrier results, *Figures 4.5* and *4.6*, considering the similarity in the results with the insulating and conducting

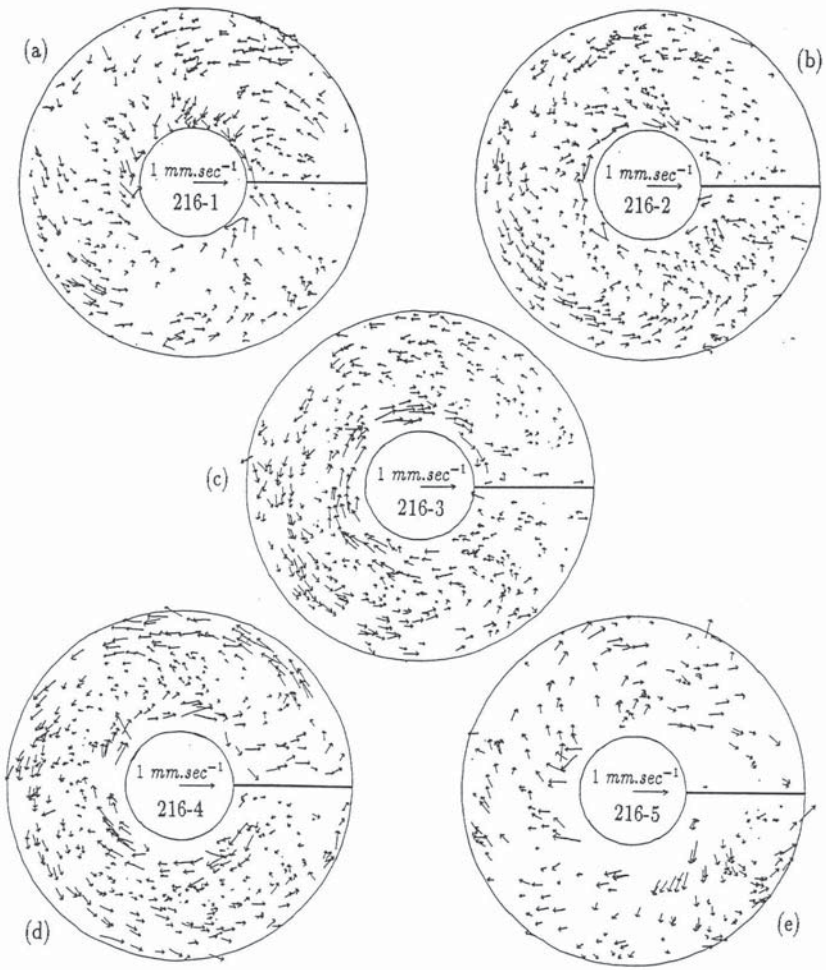

FIGURE 5.2: Horizontal velocity field data taken by VVAS, from the full radial barrier experiments for the system with constant depth, $d = 140\ mm$ (see chapter 3). The results have not been reprojected onto a regular grid to avoid any possible errors that might be caused by the least squares fitting routine. Instead each plot is a superposition of five scans at that level. The heights above the base of the annulus are: (a) 124mm, (b) 97mm, (c) 70mm, (d)43mm, and (e) 16mm. Data from run 216, $\Omega = 1.176\ rad.sec^{-1}$, $\Delta T = 4.06\ K$. These results were chosen to allow comparison with the computer simulation results.

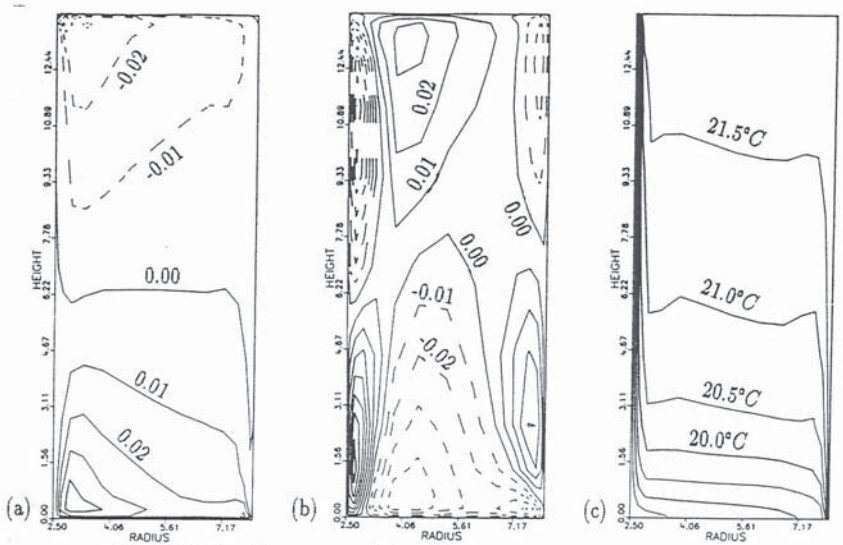

FIGURE 5.3: Computer model results from run 751, $\Omega = 1.2\ rad.sec^{-1}$, $\Delta T = 4\ K$. Cross-sections in the (r, z) plane of (a) mean radial velocity, u in $cm.sec^{-1}$, (b) mean azimuthal velocity, v in $cm.sec^{-1}$, and (c) mean fluid temperature. In (a) and (b) solid contours denote positive velocity, and dashed contours negative velocity.

barriers this is perhaps not surprising.

Spurious motions were also observed near the inner cylinder by *White (1988)*, who found that for an unblocked non-rotating annulus there were spurious time-dependent eddy motions by the inner cylinder with (r, z) grids of certain resolutions. Using unstretched $N \times N$ grids, spurious motions were observed for $N = 40$, but not for $N = 24, 32, 48, 56$, or 64. A 64×64 grid was required to give heat transport measurements which fell within the error bars of the experimental observations. He concluded that spurious eddies were seen at intermediate resolutions.

These spurious motions were only seen in the unblocked annulus when $\Omega = 0$, while *Figure 5.1* seems to show spurious motions in the simulation of the fully blocked annulus flow at $\Omega = 1.2\ rad.sec^{-1}$. However the flows observed in the

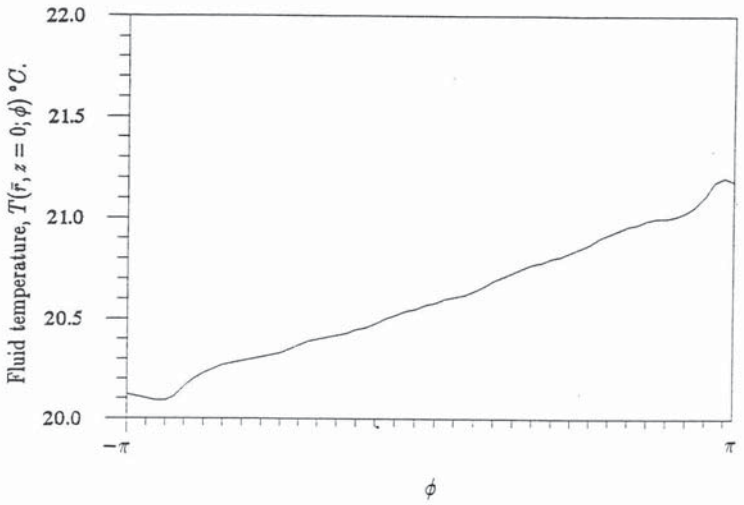

FIGURE 5.4: Computer model results from run 751, $\Omega = 1.2$ *rad.sec*$^{-1}$, and $\Delta T = 4$ *K*. Fluid temperature at $r = \bar{r}$ and $z = 0$, plotted against ϕ. The plot is chosen to allow comparison with the thermocouple ring measurements of the experiments described in chapter 3 (the full insulating barrier system). The markings along the horizontal axis have the same spacing as the thermocouples in the experiments. These results give $\Delta T_B = 1.11°C$.

blocked annulus when $\Omega \neq 0$ do have several features in common with non-rotating unblocked annulus flows, namely; a strong radial overturning cell (the η-circulation in the full barrier experiments) and a similar (r, z) temperature field. *Figure 5.5* shows the spurious eddy motions observed by *White (1988)* in simulations of unblocked annulus flows. *Figure 5.5(c)* shows the results that White obtained in a simulation of unblocked flow in an annulus at $\Omega = 0$, at $\Delta T = 4$ *K*, where the temperature and velocity fields seem fairly similar to those seen at $\Omega = 1.2$ *rad.sec*$^{-1}$ with a full radial barrier, shown in *Figure 5.3 (c)*.

Thus it seems possible that the spurious motions seen in the fully blocked simulations at $\Omega = 1.2$ *rad.sec*$^{-1}$ and $\Delta T = 4$ *K*, arise for the same reasons as

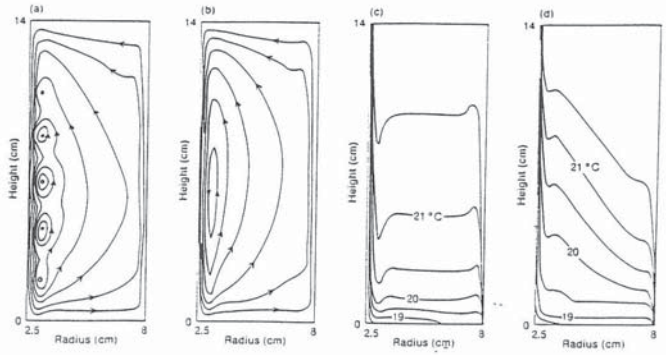

FIGURE 5.5: Cross-sections in the (r, z) plane, showing streamlines and temperature fields obtained in numerical simulations of axisymmetric annulus flow. (a) Instantaneous streamlines from an integration at $\Omega = 0$ which developed spurious eddy motion in and near the inner cylinder; 32 × 32 stretched grid. (b) Steady-state streamlines from a well-behaved integration at $\Omega = 0$; 64 × 64 unstretched grid. (In both (a) and (b) streamline contours are plotted, and the arrows indicate the direction of flow; contour interval is the same in both cases.) (c) Steady-state temperature field corresponding to (b). (d) Steady-state temperature field obtained with a 32 × 32 stretched grid (as for (a)) but at $\Omega = 0.5$ *rad.sec*$^{-1}$. In all cases the inner and outer cylinder temperatures are 17 and 21°*C*. Taken from *White (1988)*. Notice that the temperature field in *Figure 5.3* is far more similar to (c) than (d).

those seen by *White (1988)*, namely from the inadequate resolution of the grid points.

Comparing *Figures 5.1* and *5.2*, on the whole the model does not reproduce the ζ-circulation particularly well. There is some evidence of a ζ type circulation, but it occurs at a rather lower level in the model than in the experiment, and is quite weak. Since there is some sort of ζ-circulation it is possible to use the model as a test for its mechanism, but the problems mentioned above, mean that any test concerning the ζ-circulation may not be particularly decisive.

Figure 5.4 shows a simulated thermocouple ring plot, such as those given in *Figure 3.9*. While $T(\bar{r}, z = 0; \phi)$ is qualitatively similar to the experimental

results, calculation of ΔT_B for the computer simulation gives a value of $\Delta T_B = 1.11°C$ at $\Omega = 1.2\ rad.sec^{-1}$ and $\Delta T = 4\ K$. In *Table 3.2*, experimental run 5C is the nearest equivalent ($\Omega = 1.205\ rad.sec^{-1}$ and $\Delta T = 4.00\ K$), giving a result of $\Delta T_B = 0.41\ K$. Thus the model does not agree with the experimental results in this respect. The fluid heat transport in the simulation gave a Nusselt number of 11.2, which agrees with the experimentally measured value of 11.08 ± 0.16.

The rather modest agreement between the numerical and experimental results casts some doubt on the usefulness of the model. However there is sufficent agreement to make the model a useful (if not conclusive) testing ground for certain ideas concerning the ζ-circulation.

5.3 Using the model to scale the dynamical equations.

The scaling arguments applied to the equations of motion in §1.2.2 can be refined by using the numerical model to obtain the sizes of the terms in each of the components of the equation of motion as a function of position in the annulus. *Figures 5.6 – 5.8* show the sizes of each of the terms in the radial, azimuthal and vertical equations of motion against radius, azimuth and height. Providing the model is able to simulate the flow with suitable accuracy this approach should allow the significant terms in the boundary layers to be seen, as well as in the body of the fluid. This provides a check on the conclusions of §1.2.2 that azimuthal geostrophic balance and the hydrostatic equation are accurate to a good approximation.

Figure 5.6 shows sizes of the terms for the components of the equation of motion against radius. In the body of the fluid radial and azimuthal geostrophic balance can be seen to apply, and hydrostatic balance in the vertical. (a) shows that the centrifugal force term is the next most significant term after the Coriolis

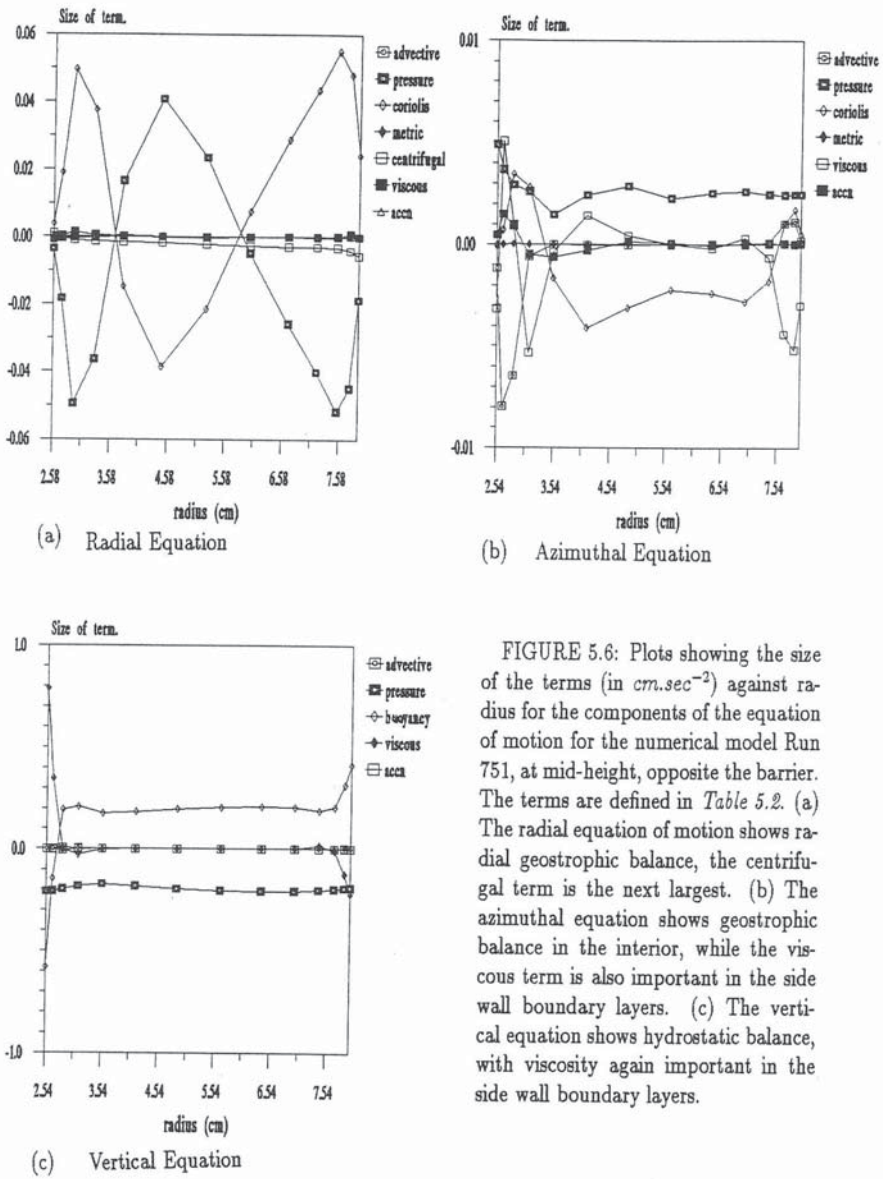

(a) Radial Equation

(b) Azimuthal Equation

(c) Vertical Equation

FIGURE 5.6: Plots showing the size of the terms (in $cm.sec^{-2}$) against radius for the components of the equation of motion for the numerical model Run 751, at mid-height, opposite the barrier. The terms are defined in *Table 5.2*. (a) The radial equation of motion shows radial geostrophic balance, the centrifugal term is the next largest. (b) The azimuthal equation shows geostrophic balance in the interior, while the viscous term is also important in the side wall boundary layers. (c) The vertical equation shows hydrostatic balance, with viscosity again important in the side wall boundary layers.

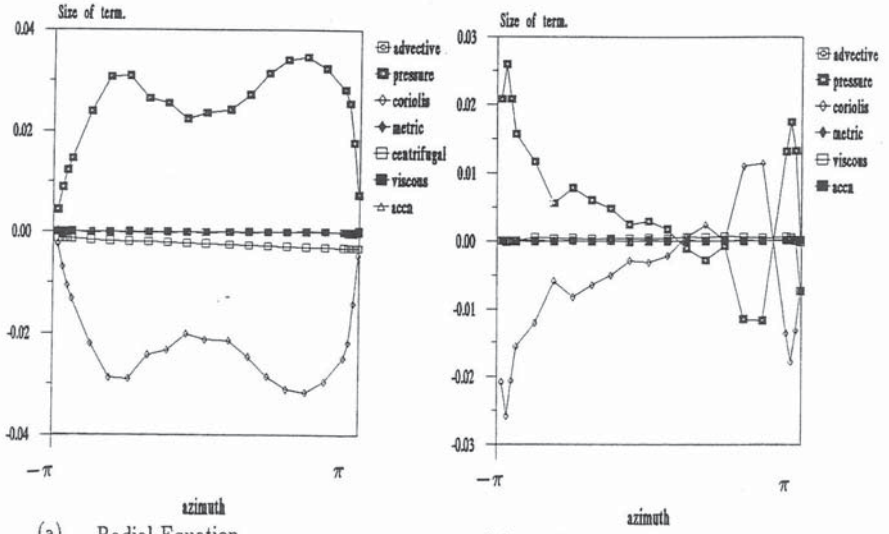

(a) Radial Equation

(b) Azimuthal Equation

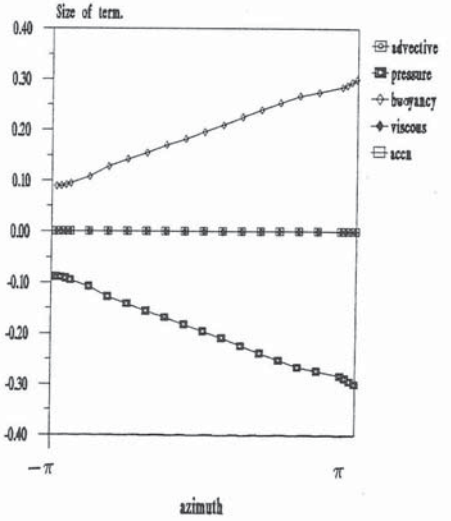

(c) Vertical Equation

FIGURE 5.7: Plots showing the size of the terms (in $cm.sec^{-2}$) against azimuth for the components of the equation of motion for the numerical model Run 751 at mid-height and mid-radius. The terms are defined in *Table 5.2.* (a) The radial equation of motion shows radial geostrophic balance, the centrifugal term is the next largest. (b) The azimuthal equation shows geostrophic balance in the interior, it is possible that there may be a boundary layer on the $\phi = \pi$ side of the barrier, but this is not matched on the other side of the barrier. (c) The vertical equation shows hydrostatic balance.

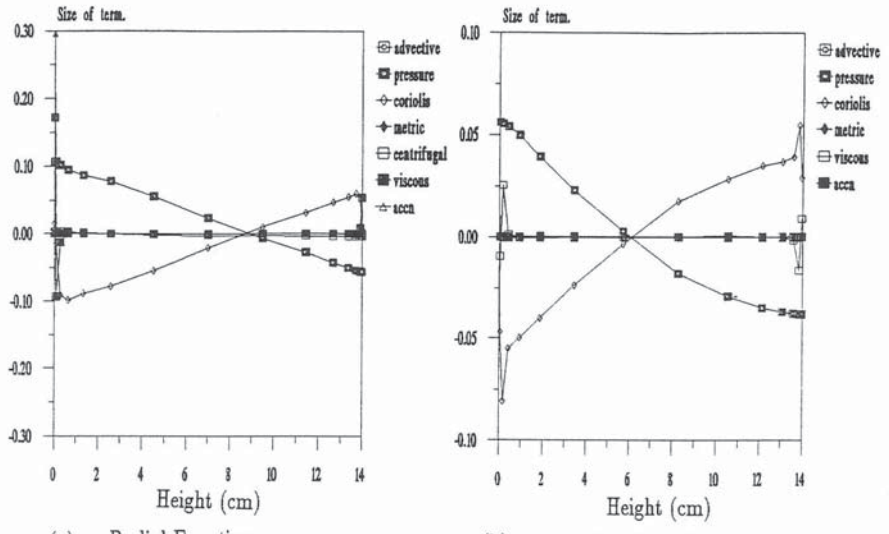

(a) Radial Equation

(b) Azimuthal Equation

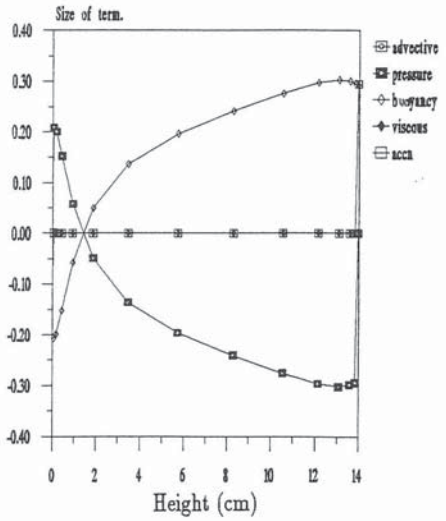

(c) Vertical Equation

FIGURE 5.8: Plots showing the size of the terms (in $cm.sec^{-2}$) against height for the components of the equation of motion for the numerical model Run 751, at mid-radius, opposite the barrier. The terms are defined in *Table 5.2.* (a) The radial equation of motion shows radial geostrophic balance. (b) The azimuthal equation shows geostrophic balance in the interior, while the viscous term is also important in the Ekman boundary layers. (c) The vertical equation shows hydrostatic balance.

Name of term	Description of term
advective	$\vec{u}.\nabla u$, $\vec{u}.\nabla v$, or $\vec{u}.\nabla w$
pressure	$\frac{1}{\bar{\rho}}\nabla p$, where p is the deviation from the reference function: $p_0 = \bar{\rho}g(d-z) + \frac{1}{2}\bar{\rho}\Omega^2 r^2$, see *Hignett et al. (1985).*
Coriolis	$2\vec{\Omega} \times \vec{u}$
metric	u^2/r or uv/r
centrifugal	$\Omega^2 \vec{r}\alpha(T - \bar{T})$
viscous	more complex than $\nu\nabla^2\vec{u}$, see *Hignett et al (1985).*
accn.	$\partial\vec{u}/\partial t$
buoyancy	$g\alpha(T - \bar{T})$

TABLE 5.2: Definition of terms used in *Figures 5.6* to *5.8.*

and pressure gradient terms, this suggests that the centrifugal force could be important in determining the flow. Given the spurious motions mentioned in §5.2 the values at small r should not be relied upon, however (b) shows that in the (outer) side wall boundary layer there is a balance between the advective, pressure gradient, Coriolis and viscous terms. (c) shows a thinner side wall boundary layer with a balance between the pressure gradient, buoyancy and viscous terms.

The sizes of the terms of the components of the equation of motion are shown plotted against ϕ in *Figure 5.7.* (a) and (b) show radial and azimuthal geostrophic balance, while the centrifugal term is the next largest term in (a) once again. (c) shows hydrostatic balance. On the whole there is little evidence of boundary layers by the sides of the barrier, apart from possibly in *Figure 5.7 (b).* This tends to support the apparently succesful omission of such a boundary layer in the theory of chapter 3. Since the model used an insulating barrier the result has no bearing on the conducting barrier case discussed in chapter 4.

Figure 5.8 shows the components of the equation of motion plotted against height. (a) and (b) again show geostrophic balance to a good degree of accuracy,

and (c) hydrostatic balance. (b) shows an Ekman boundary layer at the top and bottom of the annulus which involves a balance between the pressure gradient, Coriolis and viscous terms.

Thus the model suggests that at $\Omega = 1.2\ rad.sec^{-1}$, $\Delta T = 4\ K$ azimuthal geostrophic balance holds to a good order of accuracy, and that probably the boundary layers that form on each side of the insulating barrier cannot be resolved. This supports the scaling arguments of §1.2.2, and the omission of any kind of boundary layer by the sides of the barrier in the theory of chapter 3. The model also shows that the centrifugal force term is the next most significant after geostrophic balance, and so may be important in determining the flow.

5.4 The ζ-circulation.

5.4.1 Proposed mechanism for the ζ-circulation.

Condie and Griffiths (1989) performed a series of experiments with fluid in a rotating rectangular tank, in which the two shorter side–walls were differentially heated. They observed a horizontal circulation which had the same sense as the ζ–circulation (see chapter 3) when the cooled side–wall was near the axis of rotation. They concluded that their horizontal circulation was due to the curvature of isopotential surfaces caused by centrifugal forces. Thus it seemed possible that the centrifugal force was responsible for the ζ–circulation.

This proposed mechanism for the ζ-circulation can be interpreted in two ways. Condie and Griffiths explained that fluid close to the lid of the tank, travelling away from the heated end between isopycnal surfaces tends to be stretched in the vertical, as it approaches the axis of rotation and the isopycnal surfaces decrease in height. Conservation of potential vorticity then requires the generation of cyclonic relative vorticity. Fluid near the base of the tank moving away from the cold end experiences a similar effect, which also results in the generation of a

cyclonic circulation. In this way a circulation of the same sense as the observed ζ–circulation is set up.

The thermocouple ring temperature data given in chapter 3, allows a possibly conceptually simpler interpretation to be given to the ζ–circulation. Fluid by the cold side of the barrier will be denser than fluid by the warm side of the barrier. Consequently, providing that the radial density gradient does not prevent it, the fluid by the cold side of the barrier should be flung outwards by the centrifugal force. There will be radial inflow by the warm side of the barrier, by conservation of mass. *Figures 3.3* and *3.4* show that the ζ-circulation has radially outwards flow on the $\phi = -\pi$ side of the barrier, which *Figure 3.9* shows to be the cold side of the barrier.

As the centrifugal force increases in strength with Ω, this mechanism for the ζ-circulation also agrees with the observation that the velocity, v associated with the ζ-circulation increases with Ω, shown in *Figure 3.16* (see below).

Using the Boussinesq approximation, scaling the equation of motion gave,

$$2\vec{\Omega} \times \vec{u} \approx -\frac{1}{\bar{\rho}}\nabla p + \nabla\Phi, \tag{5.1}$$

(where the symbols have the meanings assigned to them in equation (1.6)), at suitably high Ω. Previously the centrifugal force had been neglected and the potential term written, $\nabla\Phi \approx -g\hat{z}$. Since the centrifugal force appears to be important, let,

$$\nabla\Phi = -g\hat{z} + \Omega^2\vec{r}. \tag{5.2}$$

Table 5.1 shows a scaling analysis for these two terms.

Term	Magnitude	Size
$-g\hat{z}$	g	$9.8\ m.sec^{-2}$
$\Omega^2\vec{r}$	$\Omega^2\frac{(a+b)}{2}$	$1.3\ m.sec^{-2}$

TABLE 5.1 : Scaling analysis for equation (5.2), using $r = \bar{r}$ and $\Omega = 5.0\ rad.sec^{-1}$. The result suggests that the centrifugal force might be important at high Ω.

Using equations (5.2) and (1.3) for ρ, the components of equation (5.1) are

$$-2\Omega v \approx -\frac{1}{\bar{\rho}}\frac{\partial p}{\partial r} + \Omega^2 r - \Omega^2 r\alpha(T - \bar{T}) \tag{5.3}$$

$$2\Omega u \approx -\frac{1}{\bar{\rho}r}\frac{\partial p}{\partial \phi}$$

$$0 \approx -\frac{1}{\bar{\rho}}\frac{\partial p}{\partial z} - g + g\alpha(T - \bar{T}) \tag{5.4}$$

Taking $\partial/\partial z$ of (5.3), $\partial/\partial r$ of (5.4) and substituting gives,

$$2\Omega\frac{\partial v}{\partial z} \approx g\alpha\frac{\partial T}{\partial r} + \Omega^2 r\alpha\frac{\partial T}{\partial z}, \tag{5.5}$$

so that if $\partial T/\partial r \ll \partial T/\partial z$ then

$$\frac{\partial v}{\partial z} \approx \frac{\Omega r\alpha}{2}.\frac{\partial T}{\partial z}.$$

Linearizing, using $\delta z = d$, $r = \bar{r}$ and $\Delta T_z = \Delta T$ gives,

$$v \approx \frac{\Omega(a+b)\alpha\Delta T}{4}. \tag{5.6}$$

This gives a value for the gradient $\Delta v/\Delta\Omega \approx 0.008\Delta T$ for v in $mm.sec^{-1}$ and Ω in $rad.sec^{-1}$. Comparison with *Figure 3.16* shows that this is clearly rather on the small side, though at least equation (5.6) does give a linear dependence on Ω. However the computor simulation was used to provide a more critical test of the role of the ζ-circulation in §5.4.2 below.

5.4.2 Testing the mechanism for the ζ-circulation.

If the ζ-circulation arises because of the role of the centrifugal force, then when the centrifugal force term is absent there can be no ζ-circulation. The use of a computer model allows two simulations of the flow to be run, both identical, except that one of the simulations is based upon a set of dynamical equations which has had the centrifugal force term removed from them. Assuming that the model is capable of simulating the dynamics of the system with sufficient accuracy, if the simulation with the centrifugal force term has a ζ-circulation, and the simulation without the centrifugal force does not, then the ζ-circulation must arise because of the centrifugal force. This provides a more critical test of the role of the centrifugal force than the analysis above, because in the model fewer approximations are made to the equations of motion of the system. However it is possible that inaccuracies due to the computational scheme used may be significant, such as those discussed in §5.2.

Figures 5.9 and *5.10* show a numerical simulation of the flow identical to that shown in *Figures 5.1* and *5.3* except that the centrifugal term (see *Table 5.2*) has been removed from the model. Comparison between *Figures 5.9* and *5.1*, and *Figures 5.10* and *5.3* shows that there is no appreciable difference between the two sets of results. While it is true that the numerical model did not simulate the ζ-circulation particularly well, this test provdes quite strong evidence that the centrifugal force term plays no part in the formation of the ζ-circulation. This is because a ζ-circulation (although a poor one) was produced in both cases, and the model shows that the centrifugal force does not play a significant role in the dynamics of the system at this rotation rate.

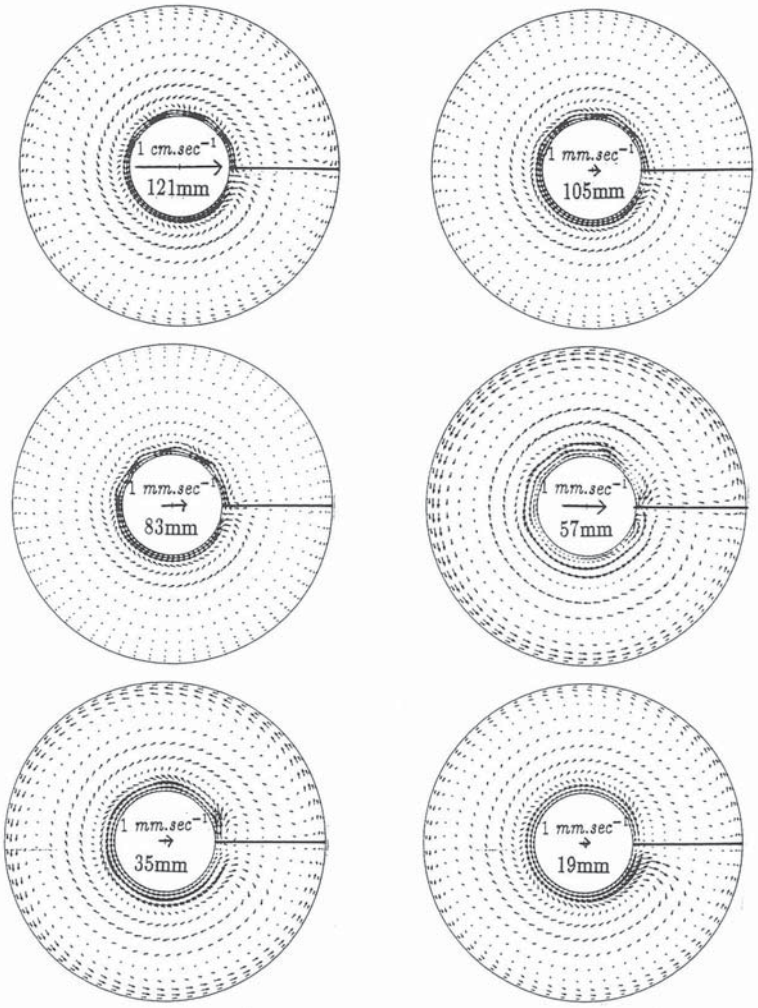

FIGURE 5.9: Computer model simulation of flow in a fully blocked annulus of constant depth, $d = 140\ mm$. Horizontal velocity results in an (r, ϕ)-plane. The solid line in the three o'clock position indicates the location of the barrier. The central arrow in each case represents a velocity of 1 $mm.sec^{-1}$, or 1 $cm.sec^{-1}$ as indicated. The heights of the (r, ϕ) cross-section above the base of the annulus are also given in the centre of each diagram. Results from run 752, the run with no centrifugal force term, $\Omega = 1.2\ rad.sec^{-1}$, $\Delta T = 4\ K$. The results are identical to those of Run 751, which included the centrifugal force.

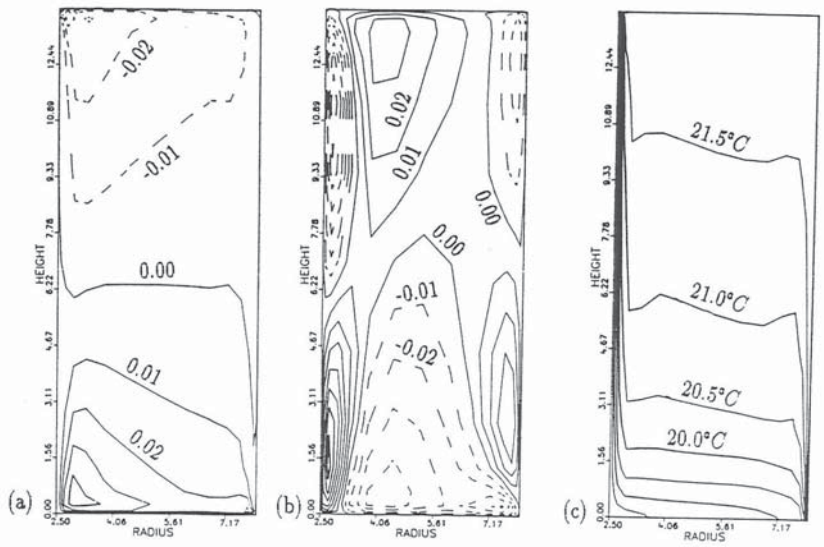

FIGURE 5.10: Computer model results from run 752, the run with no centrifugal force term, $\Omega = 1.2\ rad.sec^{-1}$, $\Delta T = 4\ K$. Cross-sections in the (r, z) plane of (a) mean radial velocity, u in $cm.sec^{-1}$, (b) mean azimuthal velocity, v in $cm.sec^{-1}$, and (c) mean fluid temperature. In (a) and (b) solid contours denote positive velocity, and dashed contours negative velocity. The results are all virtually identical to those of Run 751, which included the centrifugal force.

5.4.3 The effect of reversing ΔT.

Equation (5.5) suggests another possibility for the mechanism of the ζ-circulation, given that the centrifugal force term is unimportant, which is that v arises because of radial temperature gradients through the thermal wind equation (1.10). In other words, though $\partial T/\partial r$ is generally quite small its variation with radius is sufficient to cause the flows observed in *Figure 3.6*. This suggestion has the advantage that it can (in principle) account for the variation in v with z, though calculation of v would require detailed measurements of temperature as a function of radius. The results of D.W.Johnson (private communication) shown in

Figure 1.4(b) do suggest that the gradients are of the correct sign, and also shows the change in the sense of the gradient in $T(r)$ that would be required for $\partial v/\partial z$ to change sign with radius (see *Figure 3.6*). Since no measurements of temperature against radius were made this approach cannot be persued here. However equation (1.10) predicts that if $\partial T/\partial r$ were to change sign, $\partial v/\partial z$ should do so as well.

In order to test this idea the numerical model was run with the sense of ΔT reversed, all other model variables were kept the same. The results are shown in *Figures 5.11, 5.12* and *5.13*. *Figure 5.11* shows that the sense of the ζ-circulation has reversed, which is shown more clearly in *Figure 5.12*, which is virtually a 'mirror image' of *Figure 5.3*. These results do strongly support the idea that the ζ-circulation arises because of radial temperature variations, through the thermal wind equation (1.10).

A further result is shown in *Figure 5.13*, which is a simulated thermocouple ring plot from the model with ΔT reversed. The sense of the temperature drop across the barrier has reversed, this is to be expected, because the sign of $\partial u/\partial z$ was reversed by reversing ΔT, so that through equation (1.11), the sense of the azimuthal temperature gradient should also be reversed. However the magnitude of ΔT_B when ΔT was reversed was much less than that obtained from the model in *Figure 5.4*. This is apparently in disagreement with experimental observations with a reversed ΔT, where the magnitude of ΔT_B was found to remain unchanged (D.W.Johnson, private communication). This again suggests that the model is having difficulties in simulating the finer details of the flow.

5.5 Conclusions.

The model does not appear to be simulating the details of the flow very well, particularly near the inner cylinder. The azimuthal temperature gradient was

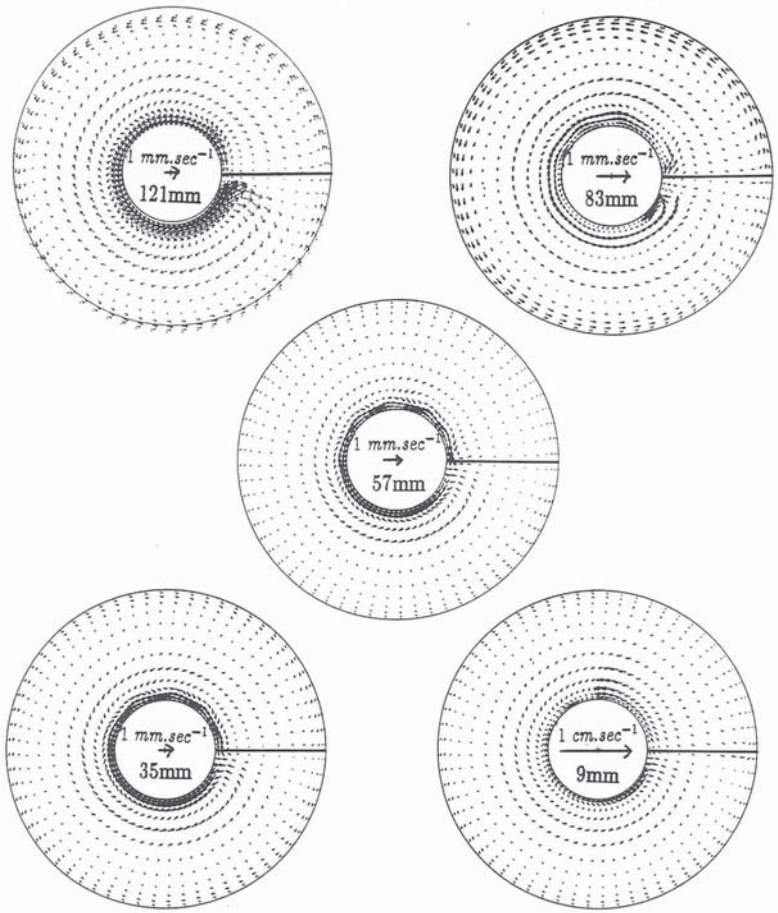

FIGURE 5.11: Computer model simulation of flow in a fully blocked annulus of constant depth, $d = 140\ mm$. Horizontal velocity results in an (r, ϕ)-plane. The solid line in the three o'clock position indicates the location of the barrier. The central arrow in each case represents a velocity of 1 $mm.sec^{-1}$, or 1 $cm.sec^{-1}$ as indicated. The heights of the (r, ϕ) cross-section above the base of the annulus are also given in the centre of each diagram. Results from run 753, the run with the reversed ΔT, $\Omega = 1.2\ rad.sec^{-1}$, $\Delta T = -4\ K$. It is easy to see that the flow by the outer wall has been reversed from Run 751, and in fact the ζ-circulation (such as it is in the model) has also been reversed.

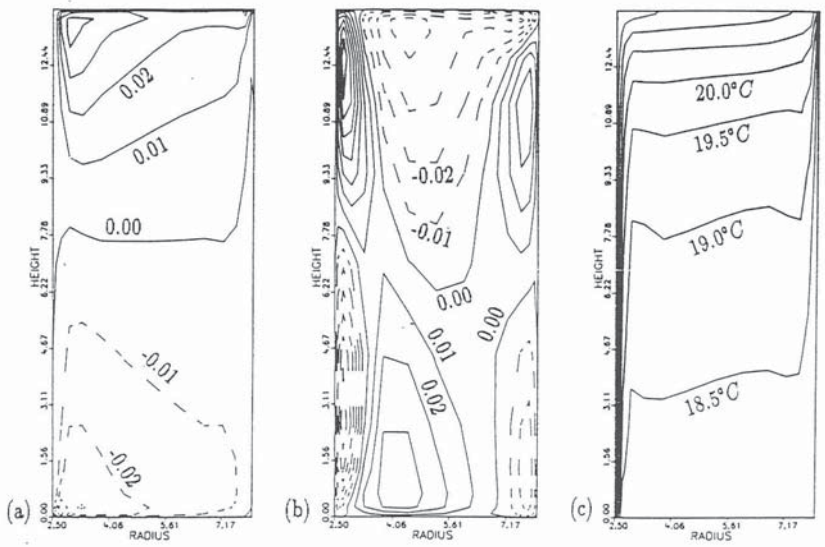

FIGURE 5.12: Computer model results from run 753, the run with the reversed ΔT, $\Omega = 1.2\ rad.sec^{-1}$, $\Delta T = -4\ K$. Cross-sections in the (r, z) plane of (a) mean radial velocity, u in $cm.sec^{-1}$, (b) mean azimuthal velocity, v in $cm.sec^{-1}$, and (c) mean fluid temperature. In (a) and (b) solid contours denote positive velocity, and dashed contours negative velocity. The sense of the η-circulation has been reversed by reversing ΔT in (a), as has the sense of v in (b), suggesting that the ζ-circulation has changed sign with ΔT also.

also much too large in the simulation. The fact that the problems appear to occur by the inner cylinder, and that the (r, z) temperature field with a barrier is quite similar to that observed in a non-rotating annulus suggest that this problem is essentially the same as that mentioned by *White (1988)*, and is due to the coarse mesh size in the model.

Section 5.3 supports the scaling arguments of §1.2.2 and indicates that there are probably no significant boundary layers to each side of the insulating barrier. However since the grid was evenly spaced in the ϕ–direction it is not clear whether the model resolution would be sufficient to show such a boundary layer. Thus

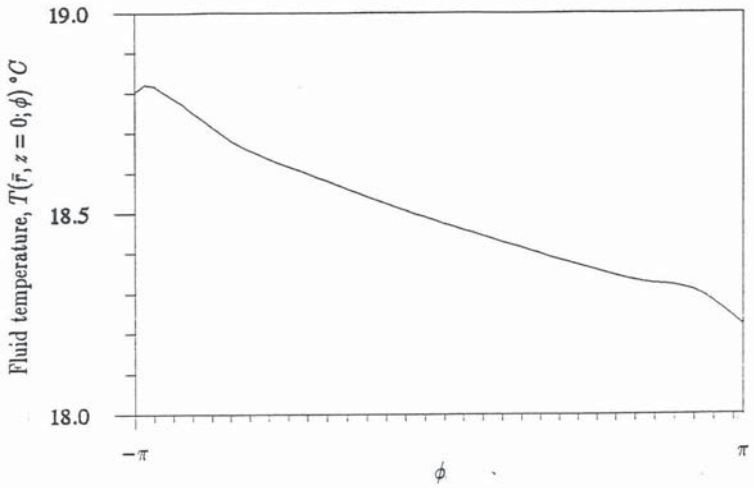

FIGURE 5.13: Computer model results from run 753, with the reversed ΔT, $\Omega = 1.2\ rad.sec^{-1}$, and $\Delta T = -4\ K$. Fluid temperature at $r = \bar{r}$ and $z = 0$, plotted against ϕ. These results give $\Delta T_B = 0.60°C$.

the use of equation (1.11) in the theory of chapter 3 is probably justified, as is the assumption that no boundary layers form by the barrier, although the evidence relating to the boundary layers is far less conclusive.

The ζ-circulation does not appear to be due to the effect of the centrifugal force, but probably to arise from small radial temperature gradients in the fluid (see equation (1.10)). Without measurements of $T(r)$ it is not possible to calculate $v(r, z)$, though qualitatively the gradients appear to be in the correct sense (see *Figures 1.4(b)* and *3.6*). While the form for the ζ-circulation suggested in §3.2.1 and *Figure 3.12* is perhaps an over simplification, it is clear that at sufficiently high Ω there must come a point where the centrifugal force term will become significant.